CHEMISTRY OF MATERIALS

pubs.acs.org/cm

Article

High-Pressure Synthesis of Bulk Cobalt Cementite, Co_3C

Paul V. Marshall, Zeynep Alptekin, Scott D. Thiel, Dean Smith, Yue Meng, and James P. S. Walsh*

Cite This: *Chem. Mater.* 2021, 33, 9601−9607

Read Online

ACCESS | Metrics & More | Article Recommendations | Supporting Information

ABSTRACT: Transition metal carbides find use in a wide range of advanced high-resilience applications including high-strength steels, heat shields, and deep-earth drills. However, carbides of the mid-to-late transition metals remain difficult to isolate and characterize on account of their metastability, which precludes the preparation of high-quality bulk single crystal samples using traditional solid-state methods. Herein, we report a combined computational and experimental survey of the cobalt−carbon binary system under high pressures and demonstrate that pressure offers a route toward the bulk synthesis of the metastable cementite-type cobalt carbide, Co_3C, which under ambient conditions can only be prepared in low-dimensional thin film or nanoparticle forms. First-principles calculations reveal two competitive low-energy stoichiometric phases under ambient pressures—*Pnnm*-Co_2C (Fe_2C-type) and *Pnma*-Co_3C (Fe_3C-type)—consistent with the known low-dimensional phases that have been studied for their promising magnetic properties. However, the calculated formation enthalpy of *Pnma*-Co_3C decreases steadily with the applied pressure, while that of *Pnnm*-Co_2C increases. We pursue these results using high-pressure laser-heated synthesis methods coupled with *in situ* X-ray diffraction and observe the formation of *Pnma*-Co_3C above 4.8 GPa. We determine the experimental bulk modulus of Co_3C to be K_0 = 237 GPa (K_p = 4.0). First-principles calculations of the phonon modes in Co_3C reveal dynamical instabilities at ambient pressure that are absent under compression. These results offer a promising new route for the synthesis of rare-earth-free magnets.

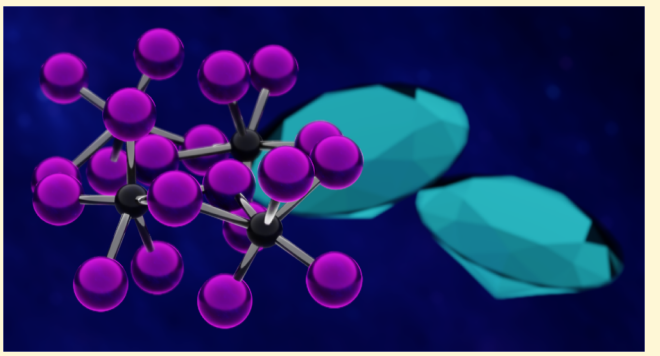

1. INTRODUCTION

Transition metal carbides (TMCs) exhibit outstanding properties across a range of applications and feature prominently in materials at the forefront of multiple industries. For example, pearlitic steel ropes used in suspension bridges owe their superlative strength properties to the presence of iron cementite, Fe_3C;[1] heat shields in hypersonic aircrafts are able to withstand extreme temperatures due to the unrivalled melting points of HfC and TaC;[2,3] and earth-boring drills can displace enormous quantities of rock owing to the extreme hardness of WC.[4] Alongside their superlative strength and resilience properties, TMCs are also heavily studied for their promising magnetic properties,[5,6] which could lead to new rare-earth-free magnets, as well as for their remarkable catalytic properties, which could lead to noble-metal-like activity using nonprecious transition metal elements.[7] MXenes, a class of two-dimensional TMCs, have exploded in popularity in recent years, being studied for a range of applications including electromagnetic interference shielding,[8] thermoelectric energy conversion,[9] and gas and pressure sensing.[10] On a more fundamental level, TMCs are also well-studied for their rich chemical bonding, which often leads to characteristics of metallic, covalent, and ionic interactions being exhibited within the same compound.[11]

TMCs of the early transition metals (groups IV−VI) readily adopt structures where the carbon atoms occupy the interstitial sites of a close-packed metal lattice (*e.g.*, HfC is an NaCl-type compound, where carbon atoms occupy the octahedral sites in the face-centered-cubic lattice of hafnium).[12,13] In these so-called interstitial compounds, the carbon atoms can form up to six M−C bonds with the surrounding metals,[14,15] leading to exceptionally high cohesion. Hägg rationalized the crystal structures observed in TMCs on the basis of the relative atomic ratio, $r = r_C/r_M$, with r = 0.59 being the cutoff where carbon atoms are no longer able to fit neatly into the interstitial sites of the metal lattice.[16] This is the main justification for why interstitial compounds are not observed beyond group VI elements,[11,17] with more complex structures—usually metal-rich—being formed instead. One example is iron cementite, Fe_3C, which is the predominant carbide in the Fe−C system.[18] Although the metal-rich carbides have a lower density of M−C bonding, they can nevertheless display remarkable bulk

Received: September 6, 2021
Revised: October 6, 2021
Published: October 21, 2021

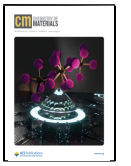

https://doi.org/10.1021/acs.chemmater.1c03092
Chem. Mater. 2021, 33, 9601−9607

properties. Indeed, a lower symmetry can confer additional benefits such as the extraordinarily high strain stiffening seen in Fe_3C.[19]

The iron cementite structure is a metastable compound formed in the production of iron steels, being produced on a scale of 50 million tons per year.[20] This structure type is also found widely in nature, with Fe_3C-type minerals being found in both meteorites originating from space and within diamond inclusions in kimberlites originating from deep within the earth's mantle.[20] However, despite the sustained interest and research effort into Fe_3C, fundamental questions concerning the mechanisms of its formation remain.[21] An outstanding issue for experimentalists has been the inability to produce high-quality synthetic samples of pure cementite,[22] stemming from the metastability of the phase and the energetically favorable decomposition into α-Fe + graphite.[23] The same metastability issues have obscured the studies of carbides in the Co−C and Ni−C systems,[24] where the even lower stability of carbide phases renders their binary phase diagrams devoid of thermodynamically stable stoichiometric compounds.[25,26]

Although the cobalt−carbide phase diagram has no stable binary compounds, two carbide phases can be stabilized in thin-film and nanoparticle forms: *Pnnm*-Co_2C (Fe_2C-type) and *Pnma*-Co_3C (cementite Fe_3C-type).[27] Both phases have been heavily studied with respect to their promising magnetic and catalytic properties.[6,28,29] Indeed, their magnetic properties are particularly exciting, with $(BH)_{max}$ values of above 20 kJ m^{-3} having been reported,[28] making these phases potentially competitive with rare-earth permanent magnets. However, the inability to prepare bulk samples has presented a roadblock to a more complete understanding of these materials. Motivated by this and encouraged by a report of pressure leading to the formation of metastable compounds in this system,[30] we investigated the Co−C system to determine whether high pressure could offer a route toward the synthesis of bulk crystalline cobalt carbides. Herein, we report the use of crystal structure prediction methods to assess the high-pressure phase space in the Co−C system, leading to the experimental laser-heated synthesis of cementite-type Co_3C above ∼5 GPa.

2. EXPERIMENTAL SECTION

2.1. Crystal Structure Prediction. Random structures were generated using the ab initio random structure searching (AIRSS) approach.[31] Structures were relaxed to their nearby minima using the geometry optimization routine in CASTEP v19.1.[32] Calculations were performed with a cutoff energy of 326.5 eV and a Monkhorst−Pack[33] grid spacing of 0.05 $Å^{-1}$. The QC5 library of pseudopotentials, which are optimized for high-throughput calculations,[32] were used in all searches. We generated between 4000−7000 structures at each pressure investigated (0−25 GPa in 5 GPa steps).

2.2. Sample Preparation. Cobalt powder (Aldrich, 2 μm, 99.98%, 0.046 g) and graphite powder (Alfa Aesar, 2−15 μm, 99.999%, 0.461 g) were loaded into a mixing jar alongside 10 zirconia spheres (10 mm diameter). This jar was then loaded into a Retsch PM100 planetary ball mill and subjected to a milling sequence consisting of 5 min intervals at 250 rpm alternating with 10 min breaks, with a total sequence time of 24 h. The ball-milled powder was pressed between two diamond anvils to produce thin flakes of roughly 5−10 μm thickness. Boehler−Almax-type diamond anvils with 300 μm culets set in tungsten carbide seats (Almax easyLab) were loaded into iBX-80 type cells (DACTools), which have a conical access of 80°. Magnesium oxide single crystals of dimensions 10 μm × 10 μm × 500 μm were polished down to a thickness of 15−20 μm and were laser-cut into discs with a diameter of 125 μm using a laser drill available to users of HPCAT, Advanced Photon Source.[34] Rhenium gaskets with a starting thickness of 250 μm were preindented to 35−40 μm. A sample space of diameter 127 μm was machined in the center of the gasket using an electrical discharge machining drill. The sample space was then loaded with a piece of the pressed Co/C flake sandwiched between two of the MgO discs.

2.3. *In Situ* Laser Heating and X-Ray Diffraction. Synthesis experiments were performed at beamline 16-ID-B at the Advanced Photon Source, Argonne National Laboratory. Samples were subjected to double-sided laser heating,[35] which we used to access temperatures up to 2000 K. Each heating run was performed on an unheated portion of the sample, at least ∼50 μm away from any prior heating runs. The incident X-rays (λ = 0.4066 Å) were aligned with the heating spot to allow for *in situ* characterization of the sample during laser heating. Pressure was increased using a single-sided gas membrane setup to allow for remote control.[36] Magnesium oxide acted as both a thermal insulator to prevent excessive heat transfer to the diamonds and a pressure standard for monitoring the pressure at the heating spot using the MgO equation of state.[37] Diffraction patterns were collected using a Pilatus 1M-F detector with 3 s exposures being automatically collected every 20 s during heating experiments. Dioptas was used for the real-time integration of the diffraction patterns.[38] TOPAS-Academic v6 was used for the Rietveld fitting of the patterns,[39,40] whose full details are provided in the Supporting Information. Strongly textured MgO reflections and diamond Bragg reflections were masked prior to the integrations used for Rietveld refinements.

2.4. First-Principles Calculations. First-principles density functional theory calculations were performed using CASTEP v19.1.[32] All calculations used the Perdew−Burke−Ernzerhof approach to the generalized gradient approximation of the exchange−correlation functional.[41] Enthalpy calculations over the 0−50 GPa range were performed using CASTEP's default "on-the-fly" generated ultrasoft psuedopotentials with a cutoff energy of 424.5 eV and a Monkhorst−Pack grid spacing of 0.03 $Å^{-1}$. The phonon dispersion of Co_3C was calculated from a relaxed structure using the supercell and finite displacement methods. These calculations used norm-conserving psuedopotentials with a cutoff energy of 1872.14 eV and a Monkhorst−Pack grid of 10 × 8 × 12.

Density of states (DOS) and phonon dispersion calculations were prepared by optimizing the geometry of Co_3C to an energy tolerance of 0.02 meV and a force tolerance of 0.01 eV $Å^{-1}$. Under the parameters of these calculations and due to the magnetic nature of cobalt, it was necessary to perform spin-polarized calculations with the spins initialized in a ferromagnetic configuration to achieve a relaxed structure. Neither a nonmagnetic nor a ferrimagnetic configuration (as in Mn_3C) was able to relax in a reasonable number (50) of iterations.[42]

Phonon calculations in CASTEP were performed with the supercell and finite displacement methods. The results of these calculations were used to compute the DOS and phonon dispersion curves interpolated along a high-symmetry path through the Brillouin zone. The path was generated using the SeeK-path tool.[43]

3. RESULTS AND DISCUSSION

3.1. Enthalpy Calculations on the Co−C System. Crystal structure prediction based on first-principles calculations is a powerful method for determining which phases are stabilized at high pressures,[31,44−46] allowing experimentalists to focus their efforts only on the regions of the phase space that show the most promise for the formation of new structures. An exhaustive survey of the high-pressure phase space—that is, the determination of the energy of every possible structure—would rely on the calculation of an intractably large potential energy surface (PES). Since this is currently not possible, various groups have devised much more efficient methods for searching for global minima on the PES.[47−49] We used the AIRSS method[31,50] coupled with the CASTEP first-principles

https://doi.org/10.1021/acs.chemmater.1c03092
Chem. Mater. 2021, 33, 9601−9607

calculations package to survey the cobalt−carbon system under high pressures.[32]

Random structures were generated and relaxed under a range of applied pressures (0−25 GPa in 5 GPa steps). The energy of each relaxed structure was used to calculate its formation enthalpy relative to the parent elements. As an illustrative example, Figure 1 plots the data generated for the

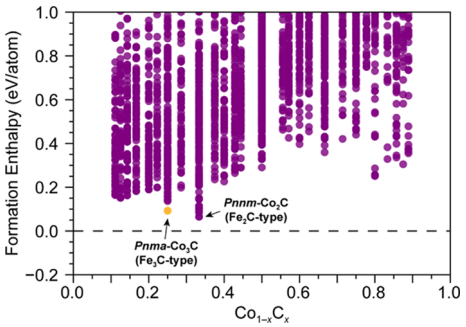

Figure 1. Calculated formation enthalpies *vs* the composition for the Co−C structures generated in the 15 GPa search. Data are cut off above 1.0 eV/atom for the improved clarity of the low-energy structures. Filled circles represent structures generated by the AIRSS search; the yellow data point represents the 16-atom *Pnma*-Co_3C structure added manually to this data set.

15 GPa search (see the Supporting Information for individual plots at each pressure). Each filled circle data point represents the formation enthalpy of a single relaxed structure. One immediate observation is that metal-rich compositions ($x < 0.5$ in $Co_{1-x}C_x$) are generally lower in energy than carbon-rich phases, consistent with the observation that compounds with a low carbon concentration are generally favored among the mid-to-late transition metals.[17] This search found the *Pnnm*-Co_2C (Fe_2C-type) structure as the lowest energy compound, with a formation enthalpy of 0.065 eV. This phase is one of the two metastable phases that have been isolated in nanoparticle and thin-film forms.[27] The other phase, *Pnma*-Co_3C (Fe_3C-type), could not be detected in this search due to the large number of atoms required to capture its primitive cell (16 atoms) *versus* the maximum number of atoms we allowed in our generated cells (9 atoms). We therefore calculated the formation enthalpy of this phase separately using the same parameters used in the searches and plotted it as a yellow data point. The *Pnma*-Co_3C phase is competitive with the Co/C 3:1 phases found in the search (see the Supporting Information). This "blind spot" in high-throughput structure searching methods toward complex structures with many atoms in their unit cell—which is ultimately imposed by finite computational resources—has motivated recent efforts to augment density functional theory calculations with machine learning methods for more efficient and expansive searches of the PES.[51−53]

The formation enthalpies of the *Pnnm*-Co_2C and *Pnma*-Co_3C phases were calculated as a function of pressure in a separate set of calculations and are plotted in Figure 2. Separate formation enthalpies are calculated using graphite-C and diamond-C as the carbon allotrope. The filled circles represent the enthalpies calculated against the lowest energy allotrope at that pressure, which is graphite between 0 and 7 GPa and diamond between 8 and 50 GPa. The plots for both *Pnnm*-Co_2C and *Pnma*-Co_3C display kinks at the crossover pressure where diamond-C becomes more stable than

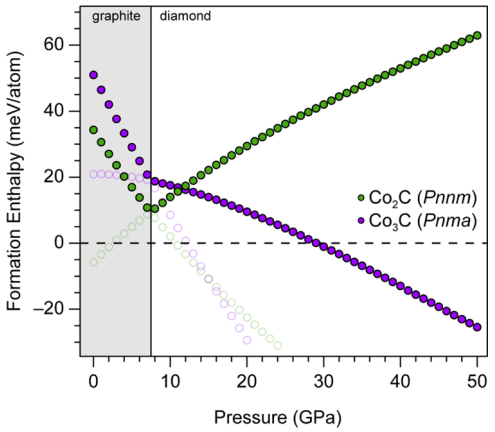

Figure 2. Plot of the calculated formation enthalpies for the *Pnnm*-Co_2C and *Pnma*-Co_3C phases between 0 and 50 GPa. The reference cobalt phase was hcp-Co over the entire pressure range, while the reference carbon phase switches from graphite to diamond between 7 and 8 GPa. Data are plotted against both carbon allotropes over the full pressure range; those using the less stable allotrope are denoted with semi-transparent open circles.

graphite-C. The positive formation enthalpies obtained at low pressures are in agreement with the experiment, where these phases are not present in the thermodynamic phase diagram. However, the accuracy of these energies should be treated with caution due to the known difficulty in capturing nonlocal dispersion interactions in graphite.[54]

The stability of the two phases respond quite differently to pressure. For *Pnnm*-Co_2C, the formation enthalpy increases with the application of pressure, while for *Pnma*-Co_3C, it drops steadily over the entire calculated pressure range. These results imply that the pressure will greatly favor the formation of *Pnma*-Co_3C while disfavoring *Pnnm*-Co_2C. The crossover to the negative formation enthalpy occurs at around 30 GPa for *Pnma*-Co_3C.

3.2. Laser-Heated Synthesis of Bulk Co_3C. Motivated by our computational results, we explored the chemical reactivity of the cobalt−carbon system between 1.1 and 13.0 GPa and with heating up to 2000 K. We used *in situ* X-ray diffraction (XRD) to monitor the crystalline phases present as we laser-heated the sample at various pressures. In our first experiment, we laser-heated our Co/C mixture slowly up to a maximum temperature of 1600 K at 1.1 GPa, observing a transformation of cobalt from hcp-Co to fcc-Co consistent with the known high-temperature behavior of this element.[55] No additional peaks were observed to form at this pressure.

At 4.8 GPa, we observed the formation of a new crystalline phase, as evidenced by the growth of reflection peaks in the integrated XRD patterns. Since we were integrating the XRD pattern in real time, we chose to hold the laser power to allow the reaction to proceed until no further changes were observed in the diffraction patterns. We then thermally quenched the reaction by turning off the lasers. We estimate a temperature of 1200 K based on fits to the emission profile. The yield of the new phase at 4.8 GPa is very low, precluding a reliable indexing of the phase. However, at a higher pressure, we observed the same peaks growing to a much higher intensity. We performed a number of heating runs over the range 5−15 GPa, all of which readily produced the same crystalline phase.

Figure 3 shows a representative pattern collected after compressing our Co/C sample to 13.0 GPa, heating to

https://doi.org/10.1021/acs.chemmater.1c03092
Chem. Mater. 2021, 33, 9601−9607

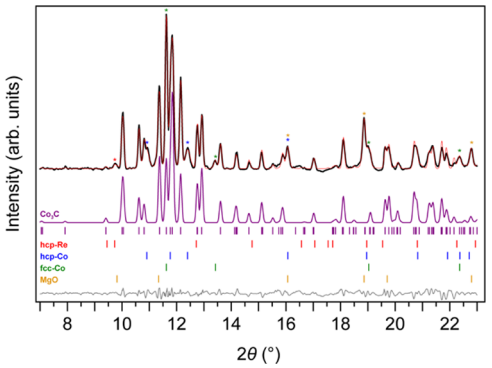

Figure 3. Powder XRD data collected after laser-heating at 13.0 GPa (black trace). The fitted trace from Rietveld refinement is plotted in red. The contribution from the Co_3C phase is plotted in purple. Additional phases included in the model are shown below the Co_3C trace, with ticks illustrating where peaks from each phase are located. Strong peaks are labeled with asterisks colored corresponding to their phase. The residual between the calculated and observed patterns is plotted in gray.

approximately 1200 K, and thermally quenching back to ambient temperature. Peaks belonging to hcp-Co and the pressure medium (MgO) are readily identified, while diffraction from graphite is not observed. The additional peaks that developed over the course of the heating belong to a single phase that indexes to an orthorhombic cell with a = 4.955 Å, b = 6.609 Å, and c = 4.40 Å. These parameters are very close to those of *Pnma*-Co_3C, and indeed, we obtain excellent fits when using this phase in Rietveld refinements (see Figure 3 and the Supporting Information).

The crystal structure of the *Pnma*-Co_3C phase is shown in Figure 4. Each unit cell contains four formula units composed

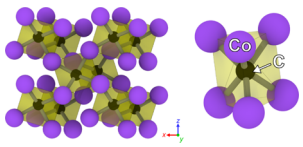

Figure 4. Crystal structure of *Pnma*-Co_3C (Fe_3C-type). Purple spheres represent cobalt and black spheres represent carbon. Trigonal prismatic coordinations around the carbon atoms are highlighted with yellow polyhedra. Image is generated using OVITO.

of four carbon atoms and 12 cobalt atoms, with each carbon atom being surrounded by six cobalt atoms in a trigonal prismatic coordination environment (illustrated with polyhedra). The structure is sometimes described as being derived from a hexagonal close-packed metal lattice. The basal layers of cobalt atoms can be viewed as zigzag folded sheets that stack as ABAB, with the atoms of one folded layer lying over the interstices of the layer below.[56] Carbon atoms then occupy the trigonal prismatic interstices in an alternating manner throughout the ABAB layers.[57]

One observation across all of the heating runs that led to Co_3C is that the carbide formation is preceded by a sharp decrease in the hcp-Co peak intensity and a concomitant increase in the fcc-Co peak intensity. This could indicate that fcc-Co is formed first above some threshold temperature and then consumed to form Co_3C through a simple diffusion mechanism. However, this seems somewhat counterintuitive given that the cobalt atoms in the cementite structure more closely resemble a distorted hcp lattice.[56,58] Computational work has shown that the interstices of both hcp and fcc cobalt are too small to allow for simple carbon diffusion into the bulk cobalt lattice and that any carbon "uptake" process is much more likely to happen via a vacancy-mediated diffusion.[59] Such a mechanism cannot be ruled out here, although the effects of pressure are likely to have a significant influence.[60]

Another interpretation of the diffraction data is that fcc-Co forms as a byproduct of the reaction hcp-Co + graphite → Co_3C, which is plausible given the uncertainty in the chemical composition of the sample flake and the possibility of a large excess of cobalt. In this interpretation, fcc-Co is not a prerequisite for the formation of Co_3C. However, it should be pointed out that a similar concomitance between the parent-element phase transitions and the onset of reactivity has been observed in other high-pressure systems.[61,62]

3.3. Experimental Compressibility of Co_3C. We used XRD to measure the unit cell of Co_3C over a range of pressure steps during decompression from 10.7 GPa. These data allow for the determination of the bulk modulus, which is a direct measure of the intrinsic resistance of a material to compression. Figure 5 plots the unit cell volume of Co_3C as

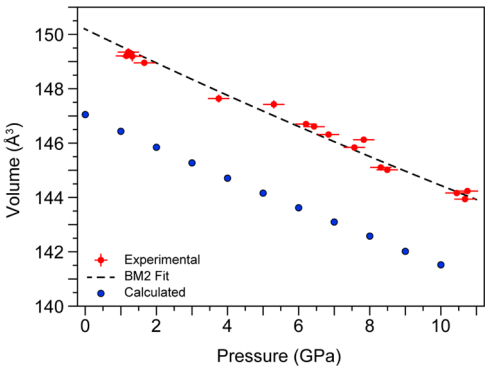

Figure 5. Plot of the experimental and calculated volumes of Co_3C as a function of pressure. Experimental data were fit to a second-order Birch–Murnaghan equation of state (dashed line) to give B_0 = 237 GPa (B_0' = 4.0 implied). Errors on the experimental data are represented with red bars.

a function of pressure. We fit these volumes to a second-order Birch–Murnaghan equation of state, from which we determine a bulk modulus (B_0) of 237 GPa (B_0' = 4.0 is implied in second-order treatments). No significant improvement in the fit was obtained with a third-order model, and in fact, these refinements yielded unrealistic highly negative values for B_0'. An F–f plot is given in the Supporting Information and suggests that B_0' does not deviate sufficiently enough from its idealized second-order value to be reliably extracted from our data. Errors in the volume of Co_3C and the pressure determined from MgO lattice parameters were derived from the estimated standard deviations of these lattice constants in our Rietveld refinements and are likely to be underestimated.[63]

A final pressure of 1.1 GPa was measured even after the mechanical force was fully removed from the diamond anvil cell (DAC). The nonhydrostaticity of the solid MgO pressure medium and the errors in the lattice spacing that this is known to cause[64] make it difficult to judge how close the final decompression point is to ambient pressure.

A value of B_0 = 237 GPa is comparable with the experimental values reported in the literature for other

https://doi.org/10.1021/acs.chemmater.1c03092
Chem. Mater. 2021, 33, 9601–9607

cementite phases Fe_3C (174 GPa)[65,66] and Mn_3C (310 GPa).[67] It also agrees well with a reported value of ∼242 GPa for Co_3C determined from first-principles methods.[68] Figure 5 plots the volumes determined from our own first-principles calculations (see Section 3.1) alongside the experimentally determined volumes. The calculated volumes are underestimated by a factor of ∼2% but show an excellent agreement with the experiment in terms of the compressibility. A third-order Birch−Murnaghan fit to the calculated data over the pressure range 0−10 GPa yields B_0 = 242.4 GPa and B_0' = 3.9, consistent with our experimental data and further justifying the use of a second-order treatment.

3.4. Dynamical Stability of Co_3C. We performed phonon dispersion calculations on Co_3C at 0 and 10 GPa to assess its dynamical stability at low and high pressures. The results of these calculations are plotted in Figure 6. The presence of imaginary frequencies in the dynamical matrix—which show up as negative frequencies in the dispersion plot—is generally an indication that the structure is dynamically unstable. These imaginary frequencies result from negative eigenvalues, which are interpreted to mean that a given perturbation will result in a decrease in the energy. In real terms, this implies that the structure will undergo a phase transition or decomposition with an infinitesimally small perturbation. However, it is important to note that these calculations do not account for anharmonic contributions arising from a nonzero temperature, which may have a significant influence on the stability of Co_3C. Figure 6 shows that at 0 GPa, the Co_3C structure exhibits a negative frequency between Γ and Z, while the dispersion plot calculated at 10 GPa exhibits no such feature. Therefore, based on our calculations, we should expect that bulk cementite-type Co_3C will not persist under ambient pressures. We did not observe the immediate decomposition of the Co_3C phase after full decompression of the DAC, although we should note that we were not able to monitor it beyond ∼15 min after the final decompression point. These results motivate future experiments investigating the metastability of this phase.

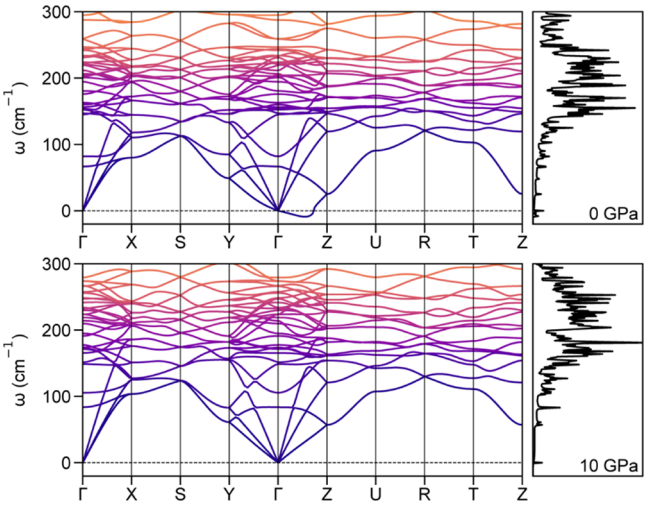

Figure 6. Dispersion plots and phonon DOS for Co_3C at 0 GPa (top) and 10 GPa (bottom). The presence of negative frequencies between Γ and Z in the 0 GPa plot indicates dynamical instability. These negative frequencies are not present in the 10 GPa calculations.

4. CONCLUSIONS

We have reported a combined computational and experimental study of the cobalt−carbon system under high pressures. First-principles calculations revealed that the formation enthalpy of the metastable cobalt cementite phase, *Pnma*-Co_3C, is reduced by the application of high pressures and eventually becomes negative. In contrast, the formation enthalpy of *Pnnm*-Co_2C, another metastable phase that is energetically competitive under ambient pressures, increases with pressure. Experimental synthesis using laser-heated DACs and *in situ* XRD confirmed these findings and allowed for the synthesis of bulk *Pnma*-Co_3C at pressures above ∼5 GPa. First-principles calculations of the phonon dispersion curves for *Pnma*-Co_3C uncovered imaginary frequencies at 0 GPa that are not present at 10 GPa, suggesting that pressure is required for *Pnma*-Co_3C to be dynamically stable. Future work will investigate the use of doping to stabilize this high-pressure phase against recovery to ambient pressures, opening the door to the elucidation of bulk electronic, magnetic, and catalytic properties of this promising family of cementite structures. These results further strengthen the case for *Pnma*-Co_3C as a competitive alternative to rare-earth-based permanent magnets.

■ ASSOCIATED CONTENT

Supporting Information

The Supporting Information is available free of charge at https://pubs.acs.org/doi/10.1021/acs.chemmater.1c03092.

XRD waterfall plots; formation enthalpy plots; experimental setup illustrations; decompression cell parameters; and Rietveld refinement details (PDF)

■ AUTHOR INFORMATION

Corresponding Author

James P. S. Walsh − *Department of Chemistry, University of Massachusetts Amherst, Amherst, Massachusetts 01003, United States;* orcid.org/0000-0003-3454-3428; Email: jpswalsh@umass.edu

Authors

Paul V. Marshall − *Department of Chemistry, University of Massachusetts Amherst, Amherst, Massachusetts 01003, United States;* orcid.org/0000-0002-8332-8591

Zeynep Alptekin − *Department of Chemistry, University of Massachusetts Amherst, Amherst, Massachusetts 01003, United States;* orcid.org/0000-0002-3018-9946

Scott D. Thiel − *Department of Chemistry, University of Massachusetts Amherst, Amherst, Massachusetts 01003, United States;* orcid.org/0000-0002-9947-0277

Dean Smith − *HPCAT, X-ray Science Division, Argonne National Laboratory, Lemont, Illinois 60439, United States;* orcid.org/0000-0001-5491-747X

Yue Meng − *HPCAT, X-ray Science Division, Argonne National Laboratory, Lemont, Illinois 60439, United States*

Complete contact information is available at: https://pubs.acs.org/10.1021/acs.chemmater.1c03092

Notes

The authors declare no competing financial interest.

■ ACKNOWLEDGMENTS

Portions of this work were performed at HPCAT (Sector 16), Advanced Photon Source (APS), Argonne National Labo-

ratory. HPCAT operations are supported by DOE-NNSA's Office of Experimental Sciences. The Advanced Photon Source is a U.S. Department of Energy (DOE) Office of Science User Facility operated for the DOE Office of Science by the Argonne National Laboratory under contract no. DE-AC02-06CH11357. This work was completed in part with resources provided by the University of Massachusetts' Green High Performance Computing Cluster (GHPCC).

REFERENCES

(1) Gavriljuk, V. G. "Decomposition of cementite in pearlitic steel due to plastic deformation". *Mater. Sci. Eng., A* **2003**, *345*, 81−89.
(2) Cedillos-Barraza, O.; Manara, D.; Boboridis, K.; Watkins, T.; Grasso, S.; Jayaseelan, D. D.; Konings, R. J.; Reece, M. J.; Lee, W. E. "Investigating the highest melting temperature materials: A laser melting study of the TaC-HfC system". *Sci. Rep.* **2016**, *6*, 37962.
(3) Ghaffari, S. A.; Faghihi-Sani, M. A.; Golestani-Fard, F.; Mandal, H. "Spark plasma sintering of TaC-HfC UHTC via disilicides sintering aids". *J. Eur. Ceram. Soc.* **2013**, *33*, 1479−1484.
(4) He, J.; Schoenung, J. M. "A review on nanostructured WC-Co coatings". *Surf. Coat. Technol.* **2002**, *157*, 72−79.
(5) Fang, C. M.; Van Huis, M. A.; Zandbergen, H. W. "Structural, electronic, and magnetic properties of iron carbide Fe_7C_3 phases from first-principles theory". *Phys. Rev. B: Condens. Matter Mater. Phys.* **2009**, *80*, 224108.
(6) Carroll, K. J.; Huba, Z. J.; Spurgeon, S. R.; Qian, M.; Khanna, S. N.; Hudgins, D. M.; Taheri, M. L.; Carpenter, E. E. "Magnetic properties of Co_2C and Co_3C nanoparticles and their assemblies". *Appl. Phys. Lett.* **2012**, *101*, 012409.
(7) Pang, J.; Sun, J.; Zheng, M.; Li, H.; Wang, Y.; Zhang, T. "Transition metal carbide catalysts for biomass conversion: A review". *Appl. Catal., B* **2019**, *254*, 510−522.
(8) Song, P.; Liu, B.; Qiu, H.; Shi, X.; Cao, D.; Gu, J. "MXenes for polymer matrix electromagnetic interference shielding composites: a review". *Compos. Commun.* **2021**, *24*, 100653.
(9) Sun, Y.; Chen, D.; Liang, Z. "Two-dimensional MXenes for energy storage and conversion applications". *Mater. Today Energy* **2017**, *5*, 22−36.
(10) Soomro, R. A.; Jawaid, S.; Zhu, Q.; Abbas, Z.; Xu, B. "A mini-review on MXenes as versatile substrate for advanced sensors". *Chin. Chem. Lett.* **2020**, *31*, 922−930.
(11) Oyama, S. T. Handbook of Heterogeneous Catalysis. *Transition Metal Carbides, Nitrides, and Phosphides*; Wiley-VCH Verlag GmbH & Co. KGaA: Weinheim, 2008; pp 342−356.
(12) Chen, J. G. "Carbide and nitride overlayers on early transition metal surfaces: preparation, characterization, and reactivities". *Chem. Rev.* **1996**, *96*, 1477−1498.
(13) Viñes, F.; Sousa, C.; Liu, P.; Rodriguez, J. A.; Illas, F. "A systematic density functional theory study of the electronic structure of bulk and (001) surface of transition-metals carbides". *J. Chem. Phys.* **2005**, *122*, 174709.
(14) Jeitschko, W.; Pottgen, R.; Hoffmann, R.-D. *Handbook of Ceramic Hard Materials*; John Wiley & Sons, Ltd, 2000; Chapter 1, pp 2−40.
(15) Wijeyesekera, S. D.; Hoffmann, R. "Transition metal carbides. A comparison of bonding in extended and molecular interstitial carbides". *Organometallics* **1984**, *3*, 949−961.
(16) Hägg, G. "Eigenschaften der Phasen von Übergangselementen in binären Systemen mit Bor, Kohlenstoff und Stickstoff". *Z. Phys. Chem.* **1929**, *6B*, 221−232.
(17) Wang, Q.; German, K. E.; Oganov, A. R.; Dong, H.; Feya, O. D.; Zubavichus, Y. V.; Murzin, V. Y. "Explaining stability of transition metal carbides-and why TcC does not exist". *RSC Adv.* **2016**, *6*, 16197−16202.
(18) Fang, C. M.; Sluiter, M.; Van Huis, M.; Ande, C.; Zandbergen, H. "Origin of predominance of cementite among iron carbides in steel at elevated temperature". *Phys. Rev. Lett.* **2010**, *105*, 055503.
(19) Jiang, C.; Srinivasan, S. G. "Unexpected strain-stiffening in crystalline solids". *Nature* **2013**, *496*, 339−342.
(20) Bhadeshia, H. K. D. H. "Cementite". *Int. Mater. Rev.* **2020**, *65*, 1−27.
(21) Ping, D.-H.; Chen, H.; Xiang, H. "Formation of θ-Fe_3C Cementite via θ'-Fe_3C (ω-Fe_3C) in Fe−C Alloys". *Cryst. Growth Des.* **2021**, *21*, 1683−1688.
(22) Terashima, T.; Tomota, Y.; Isaka, M.; Suzuki, T.; Umemoto, M.; Todaka, Y. "Strength and deformation behavior of bulky cementite synthesized by mechanical milling and plasma-sintering". *Scripta Mater.* **2006**, *54*, 1925−1929.
(23) Zhang, J.; Schneider, A.; Inden, G. "Cementite decomposition and coke gasification in He and H_2-He gas mixtures". *Corros. Sci.* **2004**, *46*, 667−679.
(24) Tokumitsu, K. "Synthesis of metastable Fe_3C, Co_3C and Ni_3C by mechanical alloying method". *Mater. Sci. Forum* **1997**, *235-238*, 127−132.
(25) Singleton, M.; Nash, P. "The C-Ni (carbon-nickel) system". *Bull. Alloy Phase Diagrams* **1989**, *10*, 121−126.
(26) Ishida, K.; Nishizawa, T. "The C-Co (carbon-cobalt) system". *J. Phase Equilib.* **1991**, *12*, 417−424.
(27) Fan, Q.; Guo, Z.; Li, Z.; Wang, Z.; Yang, L.; Chen, Q.; Liu, Z.; Wang, X. "Atomic layer deposition of cobalt carbide thin films from cobalt amidinate and hydrogen plasma". *ACS Appl. Electron. Mater.* **2019**, *1*, 444−453.
(28) Harris, V. G.; Chen, Y.; Yang, A.; Yoon, S.; Chen, Z.; Geiler, A. L.; Gao, J.; Chinnasamy, C. N.; Lewis, L. H.; Vittoria, C.; Carpenter, E. E.; Carroll, K. J.; Goswami, R.; Willard, M. A.; Kurihara, L.; Gjoka, M.; Kalogirou, O. "High coercivity cobalt carbide nanoparticles processed via polyol reaction: a new permanent magnet material". *J. Phys. D: Appl. Phys.* **2010**, *43*, 165003.
(29) Rodriguez-Gomez, A.; Holgado, J. P.; Caballero, A. "Cobalt carbide identified as catalytic site for the dehydrogenation of ethanol to acetaldehyde". *ACS Catal.* **2017**, *7*, 5243−5247.
(30) Ershova, T. P.; Kamenetskaya, D. S.; IIina, L. P. "Construction of T-P-N state diagram Co-C up to 100 kbar pressure". *Izv. Akad. Nauk SSSR, Met.* **1982**, *1*, 153−160.
(31) Pickard, C. J.; Needs, R. J. "Ab initio random structure searching". *J. Phys.: Condens. Matter* **2011**, *23*, 053201.
(32) Clark, S. J.; Segall, M. D.; Pickard, C. J.; Hasnip, P. J.; Probert, M. I. J.; Refson, K.; Payne, M. C. "First principles methods using CASTEP". *Z. Kristallogr. Cryst. Mater.* **2005**, *220*, 567−570.
(33) Monkhorst, H. J.; Pack, J. D. "Special points for Brillouin-zone integrations". *Phys. Rev. B: Solid State* **1976**, *13*, 5188.
(34) Hrubiak, R.; Sinogeikin, S.; Rod, E.; Shen, G. "The laser micromachining system for diamond anvil cell experiments and general precision machining applications at the High Pressure Collaborative Access Team". *Rev. Sci. Instrum.* **2015**, *86*, 072202.
(35) Meng, Y.; Hrubiak, R.; Rod, E.; Boehler, R.; Shen, G. "New developments in laser-heated diamond anvil cell with in situ synchrotron x-ray diffraction at High Pressure Collaborative Access Team". *Rev. Sci. Instrum.* **2015**, *86*, 072201.
(36) Sinogeikin, S. V.; Smith, J. S.; Rod, E.; Lin, C.; Kenney-Benson, C.; Shen, G. "Online remote control systems for static and dynamic compression and decompression using diamond anvil cells". *Rev. Sci. Instrum.* **2015**, *86*, 072209.
(37) Jacobsen, S. D.; Holl, C. M.; Adams, K. A.; Fischer, R. A.; Martin, E. S.; Bina, C. R.; Lin, J.-F.; Prakapenka, V. B.; Kubo, A.; Dera, P. "Compression of single-crystal magnesium oxide to 118 GPa and a ruby pressure gauge for helium pressure media". *Am. Mineral.* **2008**, *93*, 1823−1828.
(38) Prescher, C.; Prakapenka, V. B. "DIOPTAS: a program for reduction of two-dimensional X-ray diffraction data and data exploration". *High Pressure Res.* **2015**, *35*, 223−230.
(39) Perl, J.; Shin, J.; Schümann, J.; Faddegon, B.; Paganetti, H. "TOPAS: An innovative proton Monte Carlo platform for research and clinical applications". *Med. Phys.* **2012**, *39*, 6818.
(40) Faddegon, B.; Ramos-Méndez, J.; Schuemann, J.; McNamara, A.; Shin, J.; Perl, J.; Paganetti, H. "The TOPAS tool for particle

https://doi.org/10.1021/acs.chemmater.1c03092
Chem. Mater. 2021, 33, 9601−9607

simulation, a Monte Carlo simulation tool for physics, biology and clinical research". *Phys. Med.* **2020**, *72*, 114−121.
(41) Perdew, J. P.; Burke, K.; Ernzerhof, M. "Generalized gradient approximation made simple". *Phys. Rev. Lett.* **1996**, *77*, 3865.
(42) Von Appen, J.; Eck, B.; Dronskowski, R. "A density-functional study of the phase diagram of cementite-type $(Fe, Mn)_3C$ at absolute zero temperature". *J. Comput. Chem.* **2010**, *31*, 2620−2627.
(43) Hinuma, Y.; Pizzi, G.; Kumagai, Y.; Oba, F.; Tanaka, I. "Band structure diagram paths based on crystallography". *Comput. Mater. Sci.* **2017**, *128*, 140−184.
(44) Bhat, S.; Wiehl, L.; Molina-Luna, L.; Mugnaioli, E.; Lauterbach, S.; Sicolo, S.; Kroll, P.; Duerrschnabel, M.; Nishiyama, N.; Kolb, U.; Albe, K.; Kleebe, H.-J.; Riedel, R. "High-pressure synthesis of novel boron oxynitride $B_6N_4O_3$ with sphalerite type structure". *Chem. Mater.* **2015**, *27*, 5907−5914.
(45) Dewaele, A.; Worth, N.; Pickard, C. J.; Needs, R. J.; Pascarelli, S.; Mathon, O.; Mezouar, M.; Irifune, T. "Synthesis and stability of xenon oxides Xe_2O_5 and Xe_3O_2 under pressure". *Nat. Chem.* **2016**, *8*, 784−790.
(46) Altman, A. B.; Tamerius, A. D.; Koocher, N. Z.; Meng, Y.; Pickard, C. J.; Walsh, J. P. S.; Rondinelli, J. M.; Jacobsen, S. D.; Freedman, D. E. "Computationally Directed Discovery of $MoBi_2$". *J. Am. Chem. Soc.* **2020**, *143*, 214−222.
(47) John, C.; Owais, C.; James, A.; Swathi, R. S. "Swarm Intelligence Steers a Global Minima Search of Clusters Bound on Carbon Nanostructures". *J. Phys. Chem. C* **2020**, *125*, 2811−2823.
(48) Kaappa, S.; del Río, E. G.; Jacobsen, K. W. "Global optimization of atomic structures with gradient-enhanced Gaussian process regression". *Phys. Rev. B* **2021**, *103*, 174114.
(49) Paleico, M. L.; Behler, J. "A flexible and adaptive grid algorithm for global optimization utilizing basin hopping Monte Carlo". *J. Chem. Phys.* **2020**, *152*, 094109.
(50) Pickard, C. J.; Needs, R. J. "High-pressure phases of silane". *Phys. Rev. Lett.* **2006**, *97*, 045504.
(51) Deringer, V. L.; Proserpio, D. M.; Csányi, G.; Pickard, C. J. "Data-driven learning and prediction of inorganic crystal structures". *Faraday Discuss.* **2018**, *211*, 45−59.
(52) Deringer, V. L.; Pickard, C. J.; Csányi, G. "Data-driven learning of total and local energies in elemental boron". *Phys. Rev. Lett.* **2018**, *120*, 156001.
(53) Bernstein, N.; Csányi, G.; Deringer, V. L. "De novo exploration and self-guided learning of potential-energy surfaces". *npj Comput. Mater.* **2019**, *5*, 99.
(54) Mosyagin, I.; Gambino, D.; Sangiovanni, D. G.; Abrikosov, I. A.; Caffrey, N. M. "Effect of dispersion corrections on ab initio predictions of graphite and diamond properties under pressure". *Phys. Rev. B* **2018**, *98*, 174103.
(55) Yoo, C.-S.; Söderlind, P.; Cynn, H. "The phase diagram of cobalt at high pressure and temperature: the stability of γ(fcc)-cobalt and ε'(dhcp)-cobalt". *J. Phys.: Condens. Matter* **1998**, *10*, L311.
(56) Chiou, W., Jr; Carter, E. A. "Structure and stability of Fe_3C-cementite surfaces from first principles". *Surf. Sci.* **2003**, *530*, 88−100.
(57) Fasiska, E. J.; Jeffrey, G. A. "On the cementite structure". *Acta Crystallogr.* **1965**, *19*, 463−471.
(58) Cottrell, A. H. "A theory of cementite". *Mater. Sci. Technol.* **1993**, *9*, 277−280.
(59) Lizárraga, R.; Pan, F.; Bergqvist, L.; Holmström, E.; Gercsi, Z.; Vitos, L. "First Principles Theory of the hcp-fcc Phase Transition in Cobalt". *Sci. Rep.* **2017**, *7*, 3778.
(60) Ding, J.; Ye, T.; Zhang, H.; Yang, X.; Zeng, H.; Zhang, C.; Wang, X. "Pressure-induced structural phase transition and vacancy filling in titanium monoxide TiO up to 50 GPa". *Appl. Phys. Lett.* **2019**, *115*, 101902.
(61) Tamerius, A. D.; Clarke, S. M.; Gu, M.; Walsh, J. P. S.; Esters, M.; Meng, Y.; Hendon, C. H.; Rondinelli, J. M.; Jacobsen, S. D.; Freedman, D. E. "Discovery of Cu_3Pb". *Angew. Chem.* **2018**, *130*, 12991−12995.
(62) Chen, G.; Song, X.; Richardson, T. J. "Electron microscopy study of the $LiFePO_4$ to $FePO_4$ phase transition". *Electrochem. Solid-State Lett.* **2006**, *9*, A295.
(63) Haestier, J. "Handling cell errors in crystallographic data". *Crystallogr. Rev.* **2010**, *16*, 133−144.
(64) Liu, L.; Bi, Y. "How far away are accurate equations of state determinations? Some issues on pressure scales and non-hydrostaticity in diamond anvil cells". *Matter Radiat. Extremes* **2016**, *1*, 224−236.
(65) Li, J.; Mao, H. K.; Fei, Y.; Gregoryanz, E.; Eremets, M.; Zha, C. S. "Compression of Fe_3C to 30 GPa at room temperature". *Phys. Chem. Miner.* **2002**, *29*, 166−169.
(66) Scott, H. P.; Williams, Q.; Knittle, E. "Stability and equation of state of Fe_3C to 73 GPa: Implications for carbon in the Earth's core". *Geophys. Res. Lett.* **2001**, *28*, 1875−1878.
(67) Chong, X.; Jiang, Y.; Zhou, R.; Feng, J. "First principles study the stability, mechanical and electronic properties of manganese carbides". *Comput. Mater. Sci.* **2014**, *87*, 19−25.
(68) Ghosh, G. "A first-principles study of cementite (Fe_3C) and its alloyed counterparts: Elastic constants, elastic anisotropies, and isotropic elastic moduli". *AIP Adv.* **2015**, *5*, 087102.

https://doi.org/10.1021/acs.chemmater.1c03092
Chem. Mater. 2021, 33, 9601−9607